Liu, Y., et al., 2021, Archean geodynamics: Ephemeral supercontinents or long-lived supercratons: Geology, v. 49, https://doi.org/10.1130/G48575.1

Supplementary Information for

Archean geodynamics: Ephemeral supercontinents or long-lived supercratons

Yebo Liu, Ross N. Mitchell, Zheng-Xiang Li, Uwe Kirscher, Sergei A. Pisarevsky, Chong Wang

Yebo Liu
E-mail: yebo.liu@curtin.edu.au

This PDF file includes:

Supporting Information Text

Regional geology. The Yilgarn Craton is the largest Archean craton in Australia, composed of several Archean granite-greenstone terranes including the Narrayer Terrane, the Southwest Terrane, the Youanmi Terrane, and the Eastern Goldfields Superterrane (Fig. S1). While the Southwest and Narrayer terranes are mainly composed of gneiss and granite, the Youanmi Terrane and the Eastern Goldfields Superterrane are each comprised of multiple granite-greenstone belts. The ca. 3730−3300 Ma gneiss components of the Narrayer Terrane are the oldest known rocks in Yilgarn (Cassidy et al., 2006; Nutman et al., 1991; Wyche, 2007). The Narrayer and the Youanmi terranes collided ca. 2750 Ma (Cassidy et al., 2006). The South West Terrane is thought to have assembled with the Youanmi Terrane between ca. 2652-2625 Ma (Cassidy et al., 2006), which caused voluminous granite emplacement and high-grade metamorphism (Qiu et al., 1999; Wilde et al., 2002). The juxtaposition of the Eastern Goldfields Superterrane with the Youanmi Terrane happened between ca. 2678-2658 Ma (Czarnota et al., 2010; Standing, 2008). The Yilgarn Craton is bounded to the north by the Paleoproterozoic Capricorn Orogen (Johnson et al., 2011, 2013), to the west by the late Mesoproterozoic to Neoproterozoic Pinjarra Orogen (Fitzsimons, 2003; Myers et al., 1996), and to the south and southeast by the late Paleoproterozoic to Mesoproterozoic Albany-Fraser Orogen (Myers et al., 1996; Spaggiari et al., 2009, 2015, see Fig. S1).

Like other Archean cratons in the world, Yilgarn is intruded by numerous mafic dyke swarms (Fig. S1). Among them two swarms are most prominent and have already been investigated paleomagnetically: the ca. 2410 Ma Widgiemooltha dyke swarm (Evans, 1968; Smirnov et al., 2013) and the ca. 1210 Ma Marnda Moorn dyke swarm (Pisarevsky et al., 2003, 2014). Due to prolonged lateritic weathering, dykes in the Yilgarn Craton can rarely be traced in the field for more than a few kilometers (Lewis, 1994). The exception is the largely E-W trending Widgiemooltha dyke swarm transecting the Yilgarn Craton. Individual Widgiemooltha dykes can be traced, in outcrop or through magnetic anomalies, for up to 600 km. Evans (Evans, 1968) reported preliminary paleomagnetic data for the Widgiemooltha dykes, which were later improved upon with more systematic sampling and robust baked contact tests as proof of a primary magnetic remanence (Smirnov et al., 2013). The Marnda Moorn dyke swarm (including the Muggamurra, Boyagin, Wheatbelt and Gnowangerup-Fraser dykes, see Pisarevsky et al. 2003, 2014; Wang et al. 2014; Wingate and Pidgeon 2005) intrudes along multiple margins of the Yilgarn Craton except for the northeastern side, where only a small number of Marnda Moorn dykes are reported. The orientations of Marnda Moorn dykes vary widely and are generally margin-parallel. (Pisarevsky et al., 2003, 2014) reported high-quality paleomagnetic data for the Marnda Moorn dykes. Apart from these two widespread dyke swarms, three other dyke swarms with more localized occurrences were also dated and paleomagnetically studied (Fig. S1): the ca. 2401 Ma Erayinia dykes (Pisarevsky et al., 2015), the ca. 1888 Ma Boonadgin dykes (Liu et al., 2019; Stark et al., 2019) , and the ca. 1075 Ma Warakurna dykes (Wingate et al., 2004, 2002).

The recently identified 2615 ± 6 Ma Yandinilling dykes are the targets of this study. The Yandinilling dykes have consistent NE trends (Fig. S1, Table S1) with widths ranging from 1 meter to 70 meters. The Yandinilling dykes are unmetamorphosed dolerite (Stark et al., 2018) with (sub-) ophitic texture, consisting of plagioclase (45–50 vol.%), pyroxene (35–40 vol.%), and minor components of ilmenite, magnetite, quartz and apatite (Stark et al., 2018). The Yandinilling dykes intrude the metasediments, granitic gneiss, granulite and granites of the Southwest Terrane of the Yilgarn Craton (Cassidy et al., 2006, see Fig. S1). The metasedimentary and meta-igenous rocks in the study area, collectively informally named Jimperding metamorphic belt (Wilde, 2001), are formed between ca. 3.2 Ga and 2.8 Ga (Cassidy et al., 2006; Wilde, 2001). The majority of the granites in the Southwest Terrane emplaced from between ca. 2.69 Ga and ca. 2.62 Ga (Cassidy et al., 2006; Nemchin and Pidgeon, 1997; Wilde et al., 2002). The intrusion of ca. 2.64-2.62 Ga charnockitic granites was accompanied by granulite-facies metamorphism, which did not affect the Yandinilling dykes as demonstrated by Stark et al. (2018).

Sampling. A total of 123 standard 24-mm diameter cores from 15 sites were collected for rock magnetic and paleomagnetic analysis (Fig. 1). Each site represents a distinct dike. All cores were oriented using magnetic and sun compass orientations. At least one specimen per core was cut for demagnetization experiments.The host granite of 16WDS14 was also sampled for a backed contact test. The host granite sampled in this study were not prepared for geochronology. However, three geochronological samples from the same granite unit ∼50 kilometers in the east of the present sampling area yielded U-Pb zircon ages of 2659 ± 4 Ma (Lu et al., 2019a), 2662 ± 3 Ma (Lu et al., 2019b), and 2651 ± 3 Ma (Lu et al., 2019c), respectively, 35-45 Ma older than the Yandinilling dykes.

Rock magnetism. To determine the magnetic mineralogy, a set of rock magnetic experiments were conducted. Crushed powders of fresh sample materials from each site were prepared for rock magnetic analysis. Susceptibility versus temperature data were obtained using an AGICO MFK-1 Kappabridge equipped with a CS4 furnace. Hysteresis loops, IRM (isothermal remanent magnetization) acquisition and backfield demagnetization curves were measured with a Variable Field Translation Balance (Krása et al., 2007) at room temperature. Additionally, a representative selection of samples was each given a composite IRM along three orthogonal axes with magnetic fields of 2=.4 T, 0.4 T, and 0.12 T. Subsequently, the IRM-imparted samples were then subjected to stepwise thermal demagnetization (Lowrie, 1990). All the rock magnetic experiments were conducted in an air atmosphere.

The susceptibility versus temperature (κ-T) curves show a consistent sharp drop of susceptibility at 560−580 °C (Fig. S2), indicating that the main magnetic phase is very low-Ti titanomagnetite or pure magnetite. Most of the measured samples reveal broadly reversible heating and cooling curves (Fig. S2a-e), suggesting that no significant changes of magnetic mineral phases have occurred during heating. In some cases, an inflection in the heating curve between 200 °C and 300 °C is evident (Fig. S2g and h), which is a diagnostic feature of hexagonal pyrrhotite (Dunlop and Özdemir, 1997).

Repeated progressive heating experiments were performed on selected samples based on the behaviors of the one-cycle κ-T curves, the results of which can be divided into two groups. The first group exhibits reversible curves at 35−350 °C followed by continuous minor declines between 300 °C and 600 °C (Fig. S2i). The contribution of small amount of (titano)maghaemite, which is a low-temperature oxidation product of (titano)magnetite common in mafic bodies (Dunlop and Özdemir, 1997; Kirscher et al., 2019; Liu et al., 2019), inverting to haematite during heating, can explain the behavior of the first group (Dunlop and Özdemir, 1997). The second group is characterized by a distinct inflection in the 35−300 °C heating curve and a decrease between 300 and 400 °C, suggesting the presence of both pyrrhotite and (titano)maghaemite, respectively (Fig. S2j).

Demagnetization results of the three-axis IRM experiments are consistent with the κ-T analysis (Fig. S2k and m). Both low-coercivity (0−0.12 T) and medium-coercivity fractions (0.12−0.4 T) with Curie temperatures of ∼580 °C are ubiquitous in all investigated samples, confirming that the main magnetic phase is Ti-poor titanomagnetite or pure magnetite. The significant contribution of the medium-coercivity fraction also confirms the presence of SD/PSD (titano)magnetite.

Magnetic coercivities of the Yandinilling dykes determined from hysteresis loops fall between 20 mT and 30 mT, typical of titanomagnetite or magnetite (Fig. S3a and b). The open waist of the hysteresis loops indicates significant contributions of SD/PSD (titano)magnetite. Such hysteresis loops are commonly referred to as having "pot-bellied" shapes, and could be explained by a mixture of SD and superparamagnetic (SP) magnetite (Tauxe et al., 1996). IRM acquisition curves can be divided into two groups (Fig. S3c). Group 1 samples become saturated at or below fields of ∼300 mT, suggesting magnetization carried mainly by (titano)magnetite. In contrast, group 2 samples did not reach saturation until ∼500 mT, confirming the presence of pyrrhotite already revealed by thermomagnetic experiments.

In summary, rock magnetic studies demonstrate that the main magnetic phase of the Yandinilling dykes is magnetite and/or Ti-poor titanomagnetite. Prominent SD/PSD signals in most of the analyzed samples indicate that the dykes are capable of carrying stable magnetic remanence. A minor secondary magnetic phase is possibly maghaemite and/or pyrrhotite.

Paleomagnetism. Four different demagnetization procedures were used for the Yandinilling dikes. The majority of samples were subjected to progressive thermal demagnetization in 16-18 steps until the measured directions became unstable (usually between 570 and 580 °C). The rest of the samples were subjected to one of the following three demagnetization procedures: (i) AF demagnetization up to 110 mT; (ii) thermal demagnetization after AF demagnetization of 7–20 mT; (iii) thermal demagnetization after low-temperature demagnetization, i.e., liquid nitrogen immersion. Thermal demagnetization was carried out in an ASC TD-48 oven. Magnetic remanences of the samples after each demagnetization step were measured with a 2G RAPID system or an AGICO JR-6A spinner magnetometer (only when the intensity was too strong to be measured with the SQUID magnetometer). All demagnetization procedures were carried out in a magnetically shielded room. All rock magnetic and paleomagnetic analyses were conducted in the paleomagnetism laboratory at Curtin University.

Magnetization vectors were calculated using principal component analysis (Kirschvink, 1980). All vectors were calculated using at least three successive steps with a maximum angular deviation (MAD) $< 10°$. In instances where decay-to-origin or stable-endpoint behaviour was not exhibited, remagnetization great circles were used. Site-mean directions and mean virtual geomagnetic poles (VGPs) were calculated using Fisher statistics (Fisher, 1953) or the iterative approach of combining great circles and vectors (McFadden and McElhinny, 1988). All calculations were carried out using the PmagPy package (Tauxe et al., 2016). Paleogeographic reconstructions were conducted using GPlates software (Boyden et al., 2011).

Anisotropy of magnetic susceptibility (AMS). Apart from two exceptions, the degree of AMS of all the measured samples from the Yandinilling dykes is low (<1.10; Fig. S4), which is typical of mafic dykes (Khan, 1962; Tarling and Hrouda, 1993) and indicates the absence of any significant deformation after intrusion. The AMS of most dykes exhibit a foliated normal fabric (clustered K_{min} axes are orthogonal to the dyke planes while K_{max} axes are dispersed in dyke planes; see Fig. S4a). Two dykes (16WDS35 and 16WDS38) reveal lineated normal fabric (K_{max} axes are clustered in the dyke plane, Fig. S4b). When the magnetic lineation is well-developed, the direction of K_{max} is considered to represent the magma flow direction (Cañón-Tapia, 2004; Knight and Walker, 1988). The shallow inclination of the magnetic lineation of 16WDS35 and 16WDS38 implies horizontal to sub-horizontal flow, indicative of dykes being far from the magmatic centre where flow is vertical. The normal fabrics are considered to have formed during the emplacement of the magma and thus represent the primary fabric of the dykes.

The inverse fabrics (K_{max} axes perpendicular to dyke planes) were observed in three of the studied dykes (Fig. S4c), which could be explained by the single-domain effect (Ferré, 2002; Potter and Stephenson, 1988). However, other explanations such as post-intrusion alteration (Cañón-Tapia, 2004) are also possible. Identifying the cause of the inverse fabric is beyond the scope of this study, particularly as directional data do not correlate with differences in AMS data.

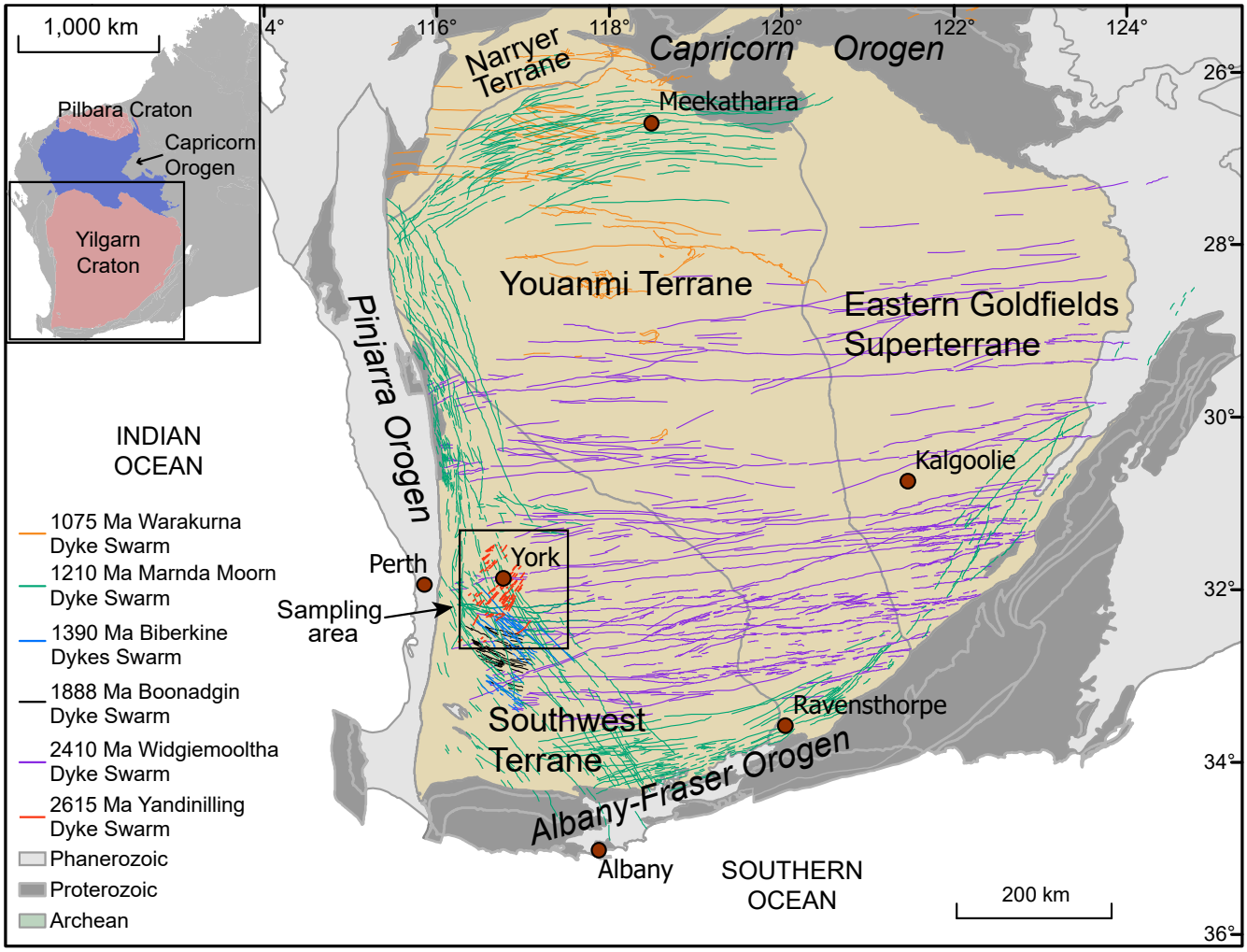

Fig. S1. Simplified geological map showing major dyke swarms (color-coded by different dyke orientation) in the Yilgarn Craton. The basemap is based on Geological Survey of Western Australia 1:2.5 M Interpreted Bedrock Geology 2015 (https://dasc.dmp.wa.gov.au/dasc).

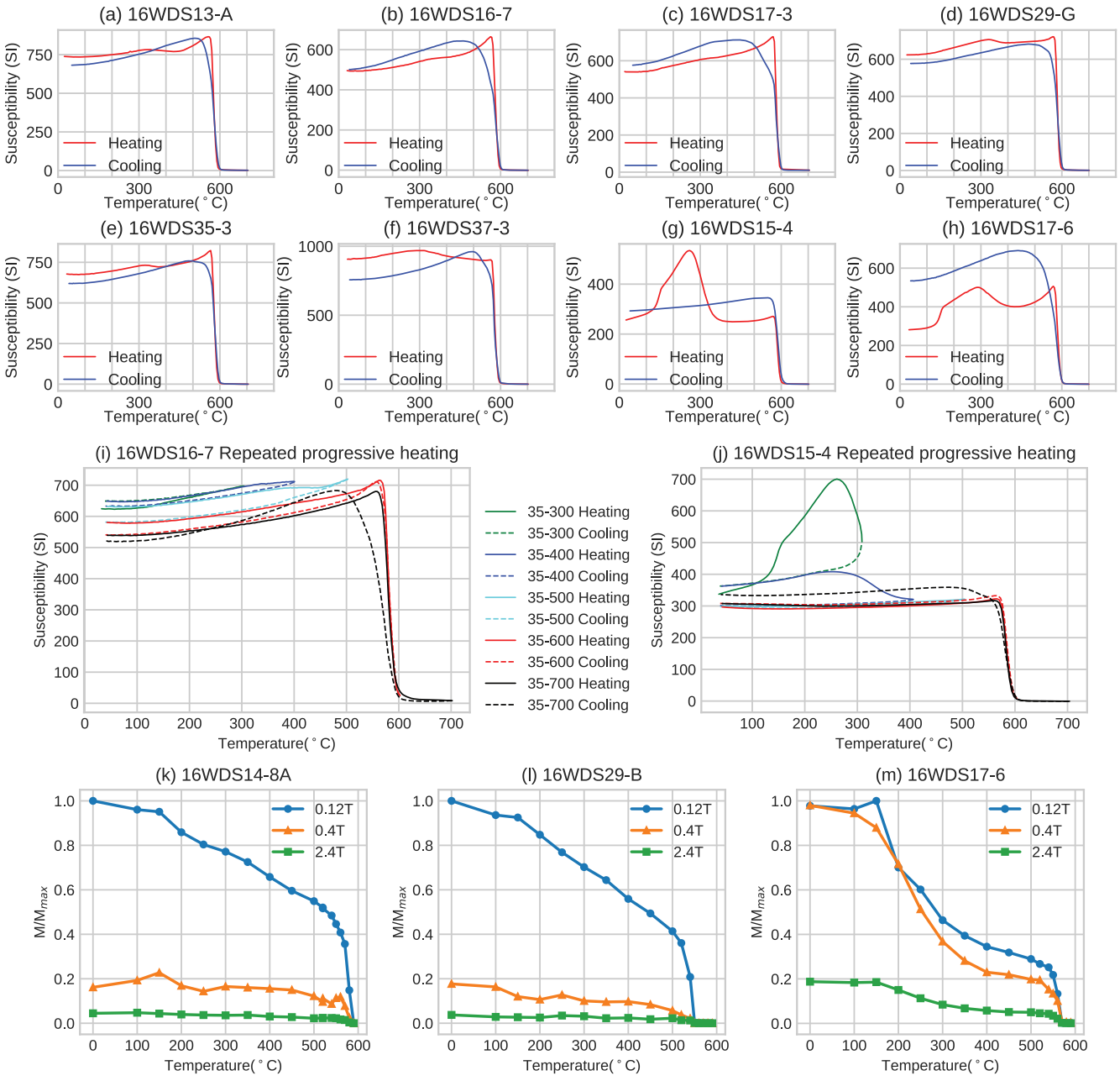

Fig. S2. Representative thermomagnetic results. (a-j) Susceptibility versus temperature curves; (k-m) Progressive thermal demagnetization of three-axis composite IRMs.

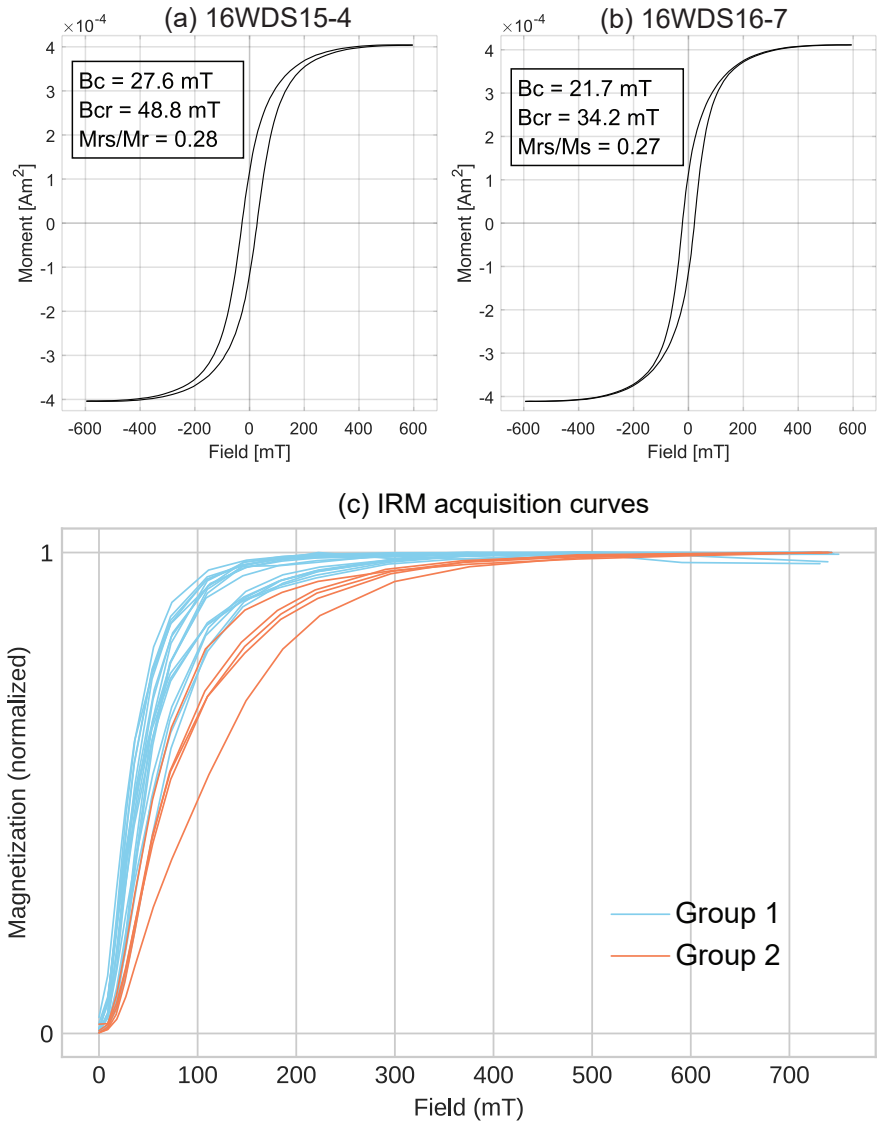

Fig. S3. (a) and (a) Representative hysteresis loops. Paramagnetic contributions are corrected; (c) IRM acquisition curves of all measured samples.

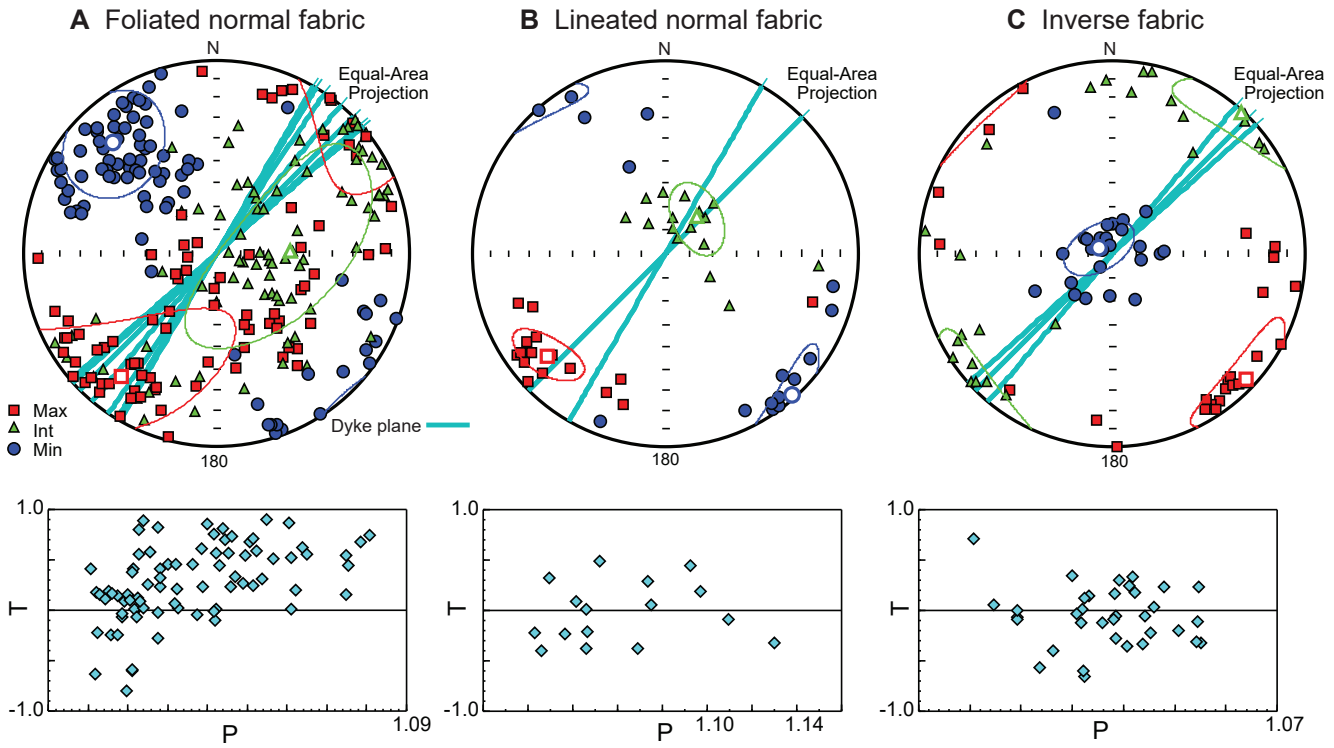

Fig. S4. Results of anisotropy of magnetic susceptibility (AMS). The upper part of the figure show AMS tensor directions of all individual samples plotted in equal-area projection divided into three different fabrics. The lower part show shape parameter (T) versus degree of anisotropy (P) corresponding to different fabrics. Dykes with (a) foliated normal fabric: 16WDS13, 16WDS15, 16WDS29, 16WDS31, 16WDS32, 16WDS33, 16WDS34, 16WDS36 and 16WDS37; (b) lineated normal fabric: 16WDS35 and 16WDS38; (c) intermediate fabric: 16WDS14, 16WDS16 and 16WDS17.

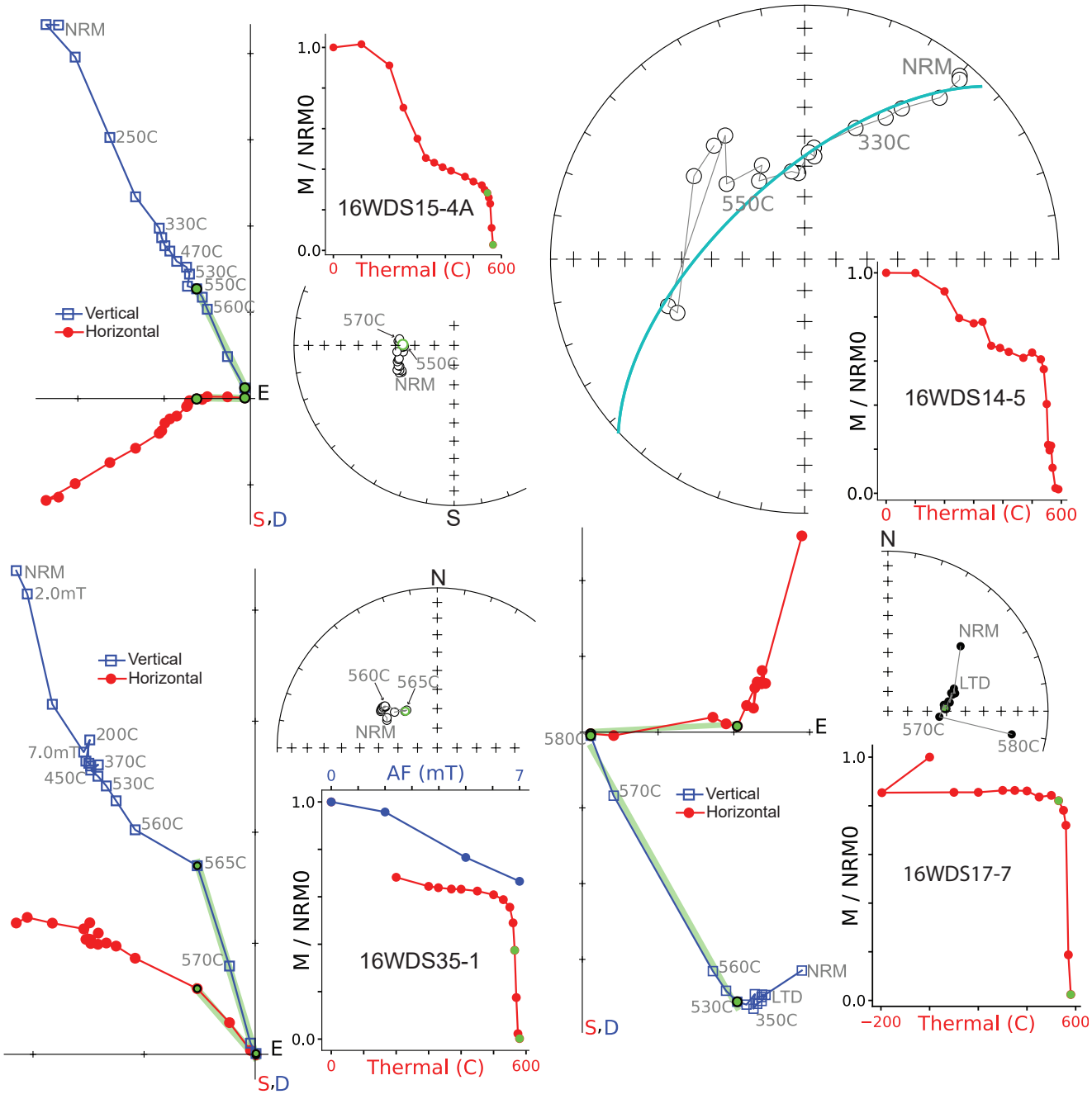

Fig. S5. Representative demagnetization plots in equal-area stereonets. Open/filled symbols indicate upper/lower hemisphere directions. NRM — natural remanent magnetization. LTD — low-temperature demagnetization.

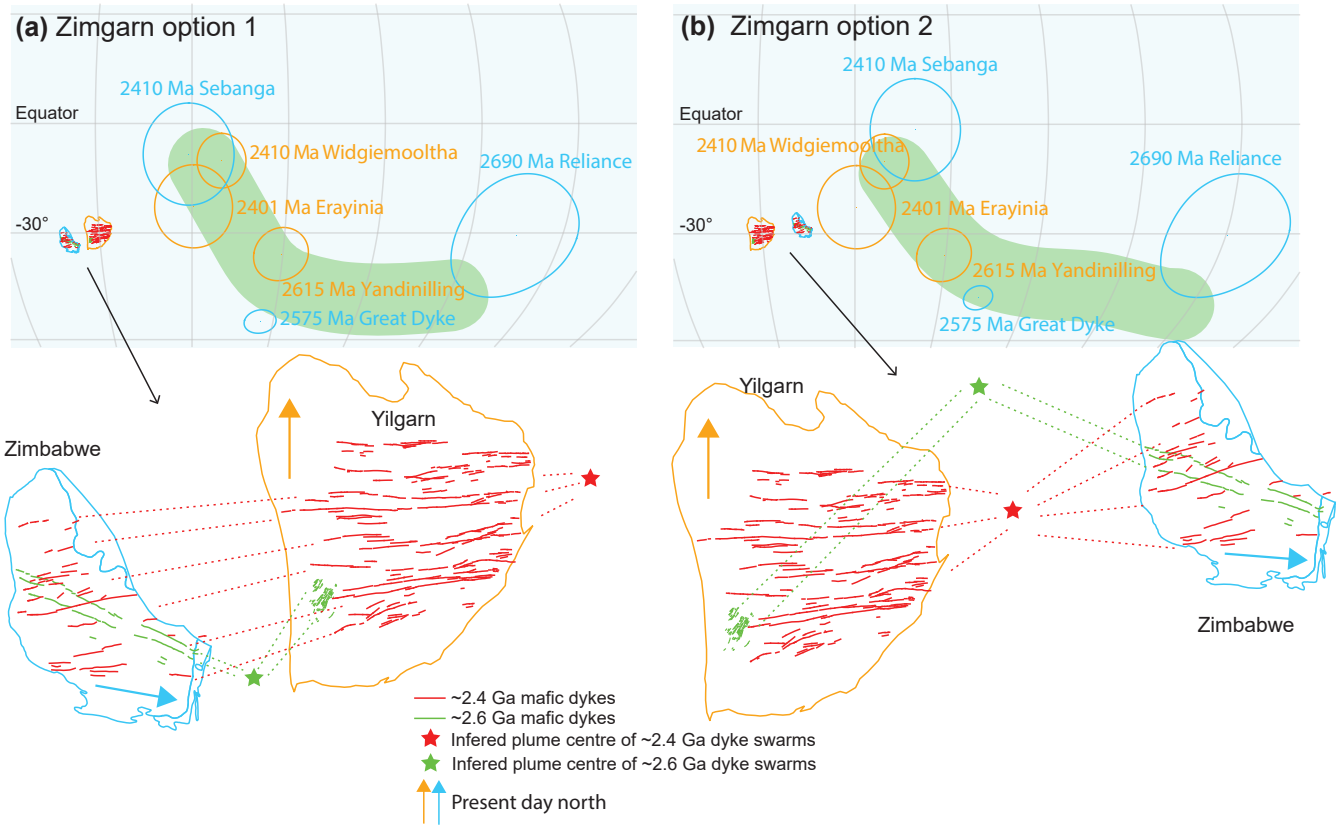

Fig. S6. Two different configurations of Zimgarn plotted in the Robinson projection along with relevant paleomagnetic poles. Zimbabwe is rotated into the Yilgarn coordinates. The green swath is a schematic illustration of the general trend of the apparent polar wander path. The lower part is the enlarged demonstration of the two configurations with inferred plume centre. (a) Zimbabwe rotated to the west side of Yilgarn using an Euler pole at 3.9°N, 70.2°W, rotation = 296.3° (Pisarevsky et al., 2015); (B) Zimbabwe rotated to the east side Yilgarn using an Euler pole at 47°S, 77°E, rotation = 157°(Smirnov et al., 2013).

Table S1. Paleomagnetic results of the 2.62 Ga Yandinilling dykes

Site (dyke)	Trend (°)	Polarity[a]	N/n	Slat. (°S)	Slong. (°E)	Dec (°)	Inc (°)	k	α_{95} (°)	Plat. (°N)	Plong. (°E)	d_p (°)	d_m (°)
16WDS13[b]	30	N	8/6	32.109628	117.151454	295.9	-51	24	15.5	36.4	9.2	14.2	21.0
16WDS14	48	N	9/8	31.585662	116.869484	277.9	-56.7	33	10	24.2	356.7	10.5	14.5
16WDS15	49	N	10/6	31.536423	116.8795	287.8	-59.6	50	9.6	32.5	356.1	10.9	14.4
16WDS16	45	N	8/7	31.878833	117.061828	300.4	-67.9	35	10.5	42.9	345	14.7	17.6
16WDS17	40	R	8/8	31.878614	117.064529	93.1	61.8	200	3.9	-23.2	169.7	4.7	6.0
16WDS29	49	N	9/9	31.572945	116.883608	292.7	-58.3	57	6.9	35.8	359	7.5	10.2
16WDS30	49	N	8/6	31.568375	116.877489	277.8	-48.5	34	11.7	21	4.4	12.7	19.0
16WDS31	48	N	8/6	31.553892	116.900216	290.9	-50.3	65	8.5	32	7.6	7.6	11.4
16WDS32[c]	40		9/6	31.578943	116.997794	121.4	29.3	7	27.7				
16WDS33[c]	45		7/6	31.6507	117.036046	268.2	-33.9	36	15				
16WDS34	31	N	7/5	31.76228	117.242068	314.6	-50.7	58	10.8	51.6	15.4	9.8	14.6
16WDS35	45	N	8/8	31.80079	117.350368	304.6	-63.9	36	9.4	45.6	352.7	11.9	15.0
16WDS36[c]	34		8/8	31.851759	117.299621	236.5	-5.4	3	35.8				
16WDS37	31	R	8/8	31.888025	117.344796	123.5	58.7	321	3.1	-44.2	181.3	3.4	4.6
16WDS38	30	R	8/8	31.888102	117.344887	133.3	61.9	102	5.6	-51.8	176.6	6.7	8.7
Mean of 12 dykes						**294.0**	**-58.1**	**72.2**	**5.1**	**36.7**	**-0.5**	**A_{95}=7.4**	

N/n = number of demagnetized/used samples; Trend = the trends of the dyke; Slat., Slon. = latitude, longitude of sample locality; Dec, Inc = site mean declination, inclination; k = precision parameter of (Fisher, 1953); α_{95} = radius of cone of 95% confidence; Plat., Plong. = latitude, longitude of the paleopole.

[a] Arbitrarily assigned, the magnetic polarity of the NW-and-up direction is referred to as normal (N) and its antipodal direction as reverse (R).

[b] Dated at 2615 ± 6 Ma by ID-TIMS U-Pb method on baddeleyite (Stark et al., 2018).

[c] Sites excluded from the calculation of mean direction.

Table S2. Paleomagnetic poles used for paleogeographic reconstructions.

Pole	Age (Ma)	Rock unit	Plat. (°N)	Plong. (°E)	A95 (°)	Reference/Source
Kola/Karelia						
Koitere	2680−2630	Koitere sanukitoid	-67.5	192.6	19.5	(Mertanen and Korhonen, 2011)
Varpaisjärvi	ca. 2600	Varpaisjärvi granulite	67.4	334.1	10	(Mertanen et al., 2006a)
KMean	ca. 2400	Karelian dykes grand mean	-16.7	250.5	8.9	Calculated by Pisarevsky (Pisarevsky et al., 2015) based on data from re
Kaapvaal						
Ongeluk	2429−2423	Ongeluk LIP grand mean	4.1	282.9	5.3	(Evans et al., 1997; Gumsley et al., 2017; Kampmann et al., 2015)
Yilgarn						
Yandinilling	2621−2610	Yandinilling dykes	36.7	-0.5	7.4	This study
Widgiemooltha	ca. 2410	Widgiemooltha dykes	10.2	339.2	7.5	(Smirnov et al., 2013)
Erayinia	2402−2400	Erayinia dykes	22.7	150.5	1.4	(Pisarevsky et al., 2015)
Zimbabwe						
Reliance	ca. 2690	Reliance middle-temp.	44	128	17	(Yoshihara and Hamano, 2004)
Great Dyke	ca. 2575	Great Dyke grand mean	24	57	9	Calculated by Smirnov (Smirnov et al., 2013) based on data from (Jones
Sebanga	ca. 2410	Sebangga Poort Dyke (VGP)	17	6.1	8	Calculated by Smirnov (Smirnov et al., 2013) based on data from (Jones
São Francisco						
Uauà	2631−2617	Uauà tholeiite dykes	25	331.4	7.4	(Salminen et al., 2019)
Slave						
Defeat	2630−2620	Defeat Suite	1.8	244.1	14.2	(Mitchell et al., 2014)

Table S3. Euler rotation parameters for Fig. 1.

Craton/block/terrane*	Euler Pole		Angle	Reference/Source
	(°N)	(°E)	(°)	
Superia				
Superior to Kola/Karelia	-75.2	50.1	273.8	Calculated from (Salminen et al., 2019)
Wyoming to Superior	48	265	125	(Kilian et al., 2016)
Hearne to Superior	60.6	227.2	89.2	Estimated from (Ernst and Bleeker, 2010)
Kaapvaal to Superior	-54.6	226.2	-223.4	Estimated from (Gumsley et al., 2017)
Pilbara to Kaapvaal	-59	251.5	93.2	(de Kock et al., 2009)
Zimgarn				
Zimbabwe to Yilgarn	43.8	244	147.9	(Pisarevsky et al., 2015)
Slave to Yilgarn	-35.8	231.7	129.1	This study
Dharwar to Slave	-49.4	53.8	256.4	Estimated from (French and Heaman, 2010)
São Francisco to Yilgarn	50.6	207.5	206.2	This study
Supercontinent ca. 2.62 Ga				
Kola/Karelia (Superia)	-76.2	217.8	102	This study
Yilgarn (Zimgarn)	16.8	232.9	-143.3	This sutdy
Supercontinent ca. 2.41 Ga				
Kola/Karelia (Superia)	-73	187.6	97.7	This study
Yilgarn (Zimgarn)	23.2	200.8	-154	This sutdy
Supercratons ca. 2.62 Ga				
Kola/Karelia (Superia)	-71.6	258.3	105	This study
Yilgarn (Zimgarn)	16.8	172.9	-143.3	This sutdy
Supercratons ca. 2.41 Ga				
Kola/Karelia (Superia)	-47.5	283.4	128.2	This study
Yilgarn (Zimgarn)	15.3	226.4	-112.6	This sutdy

* Rotation relative to absolute framework unless otherwise stated.

References

Boyden, J. A., Müller, R. D., Gurnis, M., Torsvik, T. H., Clark, J. A., Turner, M., Ivey-Law, H., Watson, R. J., and Cannon, J. S., 2011, Next-generation plate-tectonic reconstructions using GPlates: *In* Keller, G. R. and Baru, C., eds., Geoinformatics, Cambridge University Press, Cambridge, pp. 95–114, .

Cañón-Tapia, E., 2004, Anisotropy of magnetic susceptibility of lava flows and dykes: A historical account: Geological Society, London, Special Publications, vol. 238, pp. 205–225, .

Cassidy, K. F., Champion, D. C., Krapez, B., Barley, M. E., Brown, S. J. A., Blewett, R. S., Groenewald, P. B., and Tyler, I. M., 2006, A Revised Geological Framework for the Yilgarn Craton, Western Australia: Geological Survey of Western Australia – Record 2006/8: .

Czarnota, K., Champion, D. C., Goscombe, B., Blewett, R. S., Cassidy, K. F., Henson, P. A., and Groenewald, P. B., 2010, Geodynamics of the eastern Yilgarn Craton: Precambrian Research, vol. 183, pp. 175–202, .

de Kock, M. O., Evans, D. A. D., and Beukes, N. J., 2009, Validating the existence of Vaalbara in the Neoarchean: Precambrian Research, vol. 174, pp. 145–154, .

Dunlop, D. J. and Özdemir, Ö., 1997, Rock Magnetism: Cambridge University Press, Cambridge, .

Ernst, R. E. and Bleeker, W., 2010, Large igneous provinces (LIPs), giant dyke swarms, and mantle plumes: Significance for breakup events within Canada and adjacent regions from 2.5 Ga to the Present: Canadian Journal of Earth Sciences, vol. 47, pp. 695–739, .

Evans, D. A. D., Beukes, N. J., and Kirschvink, J. L., 1997, Low-latitude glaciation in the Palaeoproterozoic era: Nature, vol. 386, pp. 262–266, .

Evans, M. E., 1968, Magnetization of dikes: A study of the paleomagnetism of the Widgiemooltha Dike Suite, western Australia: Journal of Geophysical Research, vol. 73, pp. 3261–3270, .

Ferré, E. C., 2002, Theoretical models of intermediate and inverse AMS fabrics: Geophysical Research Letters, vol. 29, p. 1127, .

Fisher, R., 1953, Dispersion on a Sphere: *In* Proceedings of the Royal Society A: Mathematical, Physical and Engineering Sciences, The Royal Society, vol. 217, pp. 295–305, .

Fitzsimons, I. C. W., 2003, Proterozoic basement provinces of southern and southwestern Australia, and their correlation with Antarctica: Geological Society, London, Special Publications, vol. 206, pp. 93–130, .

French, J. E. and Heaman, L. M., 2010, Precise U-Pb dating of Paleoproterozoic mafic dyke swarms of the Dharwar craton, India: Implications for the existence of the Neoarchean supercraton Sclavia: Precambrian Research, vol. 183, pp. 416–441, .

Gumsley, A. P., Chamberlain, K. R., Bleeker, W., Söderlund, U., de Kock, M. O., Larsson, E. R., and Bekker, A., 2017, Timing and tempo of the Great Oxidation Event: Proceedings of the National Academy of Sciences, vol. 114, pp. 1811–1816, .

Johnson, S. P., Sheppard, S., Rasmussen, B., Wingate, M. T. D., Kirkland, C. L., Muhling, J. R., Fletcher, I. R., and Belousova, E. A., 2011, Two collisions, two sutures: Punctuated pre-1950Ma assembly of the West Australian Craton during the Ophthalmian and Glenburgh Orogenies: Precambrian Research, vol. 189, pp. 239–262, .

Johnson, S. P., Thorne, A. M., Tyler, I. M., Korsch, R. J., Kennett, B. L., Cutten, H. N., Goodwin, J., Blay, O., Blewett, R. S., Joly, A., Dentith, M. C., Aitken, A. R., Holzschuh, J., Salmon, M., Reading, A., Heinson, G., Boren, G., Ross, J., Costelloe, R. D., and Fomin, T., 2013, Crustal architecture of the Capricorn Orogen, Western Australia and associated metallogeny: Australian Journal of Earth Sciences, vol. 60, pp. 681–705, .

Jones, D. L., Robertson, I. D. M., and McFadden, P. L., 1975, A Paleomagnetic Study of Precambrian Dyke Swarms Associated with the Great Dyke of Rhodesia: Transactions of the Geological Society of South Africa, vol. 78, pp. 57–65.

Kampmann, T. C., Gumsley, A. P., de Kock, M. O., and Söderlund, U., 2015, U-Pb geochronology and paleomagnetism of the Westerberg Sill Suite, Kaapvaal Craton - Support for a coherent Kaapvaal-Pilbara Block (Vaalbara) into the Paleoproterozoic?: Precambrian Research, vol. 269, pp. 58–72, .

Khan, M. A., 1962, The anisotropy of magnetic susceptibility of some igneous and metamorphic rocks: Journal of Geophysical Research, vol. 67, pp. 2873–2885, .

Kilian, T. M., Bleeker, W., Chamberlain, K. R., Evans, D. A. D., and Cousens, B., 2016, Palaeomagnetism , geochronology and geochemistry of the Palaeoproterozoic Rabbit Creek and Powder River dyke swarms : Implications for Wyoming in supercraton Superia: Geological Society, London, Special Publications, vol. 424, pp. 15–45, .

Kirscher, U., Liu, Y., Li, Z., Mitchell, R., Pisarevsky, S., Denyszyn, S., and Nordsvan, A., 2019, Paleomagnetism of the Hart Dolerite (Kimberley, Western Australia) – A two-stage assembly of the supercontinent Nuna?: Precambrian Research, vol. 329, pp. 170–181, .

Kirschvink, J. L., 1980, The least-squares line and plane and the analysis of palaeomagnetic data: Geophysical Journal of the Royal Astronomical Society, vol. 62, pp. 699–718, .

Knight, M. D. and Walker, G. P. L., 1988, Magma flow directions in dikes of the Koolau Complex, Oahu, determined from magnetic fabric studies: Journal of Geophysical Research, vol. 93, p. 4301, .

Krása, D., Petersen, K., and Petersen, N., 2007, Variable Field Translation Balance: *In* Gubbins, D. and Herrero-Bervera, E., eds., Encyclopedia of Geomagnetism and Paleomagnetism, Springer Netherlands, Dordrecht, pp. 977–979, .

Lewis, J. D., 1994, Mafic dykes in the Williams–Wandering area, Western Australia: Tech. rep., Geol Surv. W. Aust.

Liu, Y., Li, Z.-X., Pisarevsky, S., Kirscher, U., Mitchell, R. N., and Stark, J. C., 2019, Palaeomagnetism of the 1.89 Ga Boonadgin dykes of the Yilgarn Craton: Possible connection with India: Precambrian Research, vol. 329, pp. 211–223, .

Lowrie, W., 1990, Identification of ferromagnetic minerals in a rock by coercivity and unblocking temperature properties:

Geophysical Research Letters, vol. 17, pp. 159–162, .
Lu, Y., Wingate, M. T. D., and Smithies, R. H., 2019a, 224404: Alkali feldspar syenite, Coarin Rock; Geochronology Record 1596: Tech. rep., Geological Survey of Western Australia.
Lu, Y., Wingate, M. T. D., and Smithies, R. H., 2019b, 224410: Granodiorite, Morrison Road; Geochronology Record 1590: Tech. rep., Geological Survey of Western Australia.
Lu, Y., Wingate, M. T. D., and Smithies, R. H., 2019c, 224412: Metagranodiorite, Doodlakine; Geochronology Record 1597: Tech. rep., Geological Survey of Western Australia.
McElhinny, M. W. and Gough, D. I., 1963, The Palaeomagnetism of the Great Dyke of Southern Rhodesia: Geophysical Journal International, vol. 7, pp. 287–303, .
McFadden, P. L. and McElhinny, M. W., 1988, The combined analysis of remagnetization circles and direct observations in palaeomagnetism: Earth and Planetary Science Letters, vol. 87, pp. 161–172, .
Mertanen, S., Hölttä, P., Paavola, J., and Pesonen, L., 2006a, Palaeomagnetism of Palaeoproterozoic dolerite dykes in central Finland: *In* Dyke Swarms - Time Markers of Crustal Evolution, Taylor & Francis, 1996, pp. 243–256, .
Mertanen, S. and Korhonen, F., 2011, Paleomagnetic constraints on an Archean–Paleoproterozoic Superior–Karelia connection: New evidence from Archean Karelia: Precambrian Research, vol. 186, pp. 193–204, .
Mertanen, S., Vuollo, J., Huhma, H., ARESTOVA, N., and Kovalenko, A., 2006b, Early Paleoproterozoic–Archean dykes and gneisses in Russian Karelia of the Fennoscandian Shield—New paleomagnetic, isotope age and geochemical investigations: Precambrian Research, vol. 144, pp. 239–260, .
Mitchell, R. N., Bleeker, W., Breemen, O. V., Lecheminant, T. N., Peng, P., Nilsson, M. K., and Evans, D. A. D., 2014, Plate tectonics before 2.0 Ga: Evidence from paleomagnetism of cratons within supercontinent nuna: American Journal of Science, vol. 314, pp. 878–894, .
Mushayandebvu, M., Jones, D., and Briden, J., 1994, A palaeomagnetic study of the Umvimeela Dyke, Zimbabwe: Evidence for a Mesoproterozoic overprint: Precambrian Research, vol. 69, pp. 269–280, .
Mushayandebvu, M. F., Jones, D. L., and Briden, J. C., 1995, Palaeomagnetic and geochrono- logical results from Proterozoic mafic intrusions in southern Zimbabwe: *In* Baer, G. and Heimann, A., eds., Physics and Chemistry of Dykes, Balkema, Rotterdam, pp. 293–303.
Myers, J. S., Shaw, R. D., and Tyler, I. M., 1996, Tectonic evolution of Proterozoic Australia: Tectonics, vol. 15, pp. 1431–1446, .
Nemchin, A. A. and Pidgeon, R. T., 1997, Evolution of the darling range batholith, Yilgarn Craton, Western Australia: A SHRIMP zircon study: Journal of Petrology, vol. 38, pp. 625–649, .
Nutman, A. P., Kinny, P. D., Compston, W., and Williams, I. S., 1991, SHRIMP U-Pb zircon geochronology of the Narryer Gneiss Complex, Western Australia: Precambrian Research, vol. 52, pp. 275–300, .
Pisarevsky, S. A., De Waele, B., Jones, S., Söderlund, U., and Ernst, R. E., 2015, Paleomagnetism and U-Pb age of the 2.4Ga Erayinia mafic dykes in the south-western Yilgarn, Western Australia: Paleogeographic and geodynamic implications: Precambrian Research, vol. 259, pp. 222–231, .
Pisarevsky, S. A., Wingate, M. T. D., and Harris, L. B., 2003, Late Mesoproterozoic (ca 1.2 Ga) palaeomagnetism of the Albany-Fraser orogen: No pre-Rodinia Australia-Laurentia connection: Geophysical Journal International, vol. 155, pp. F6–F11, .
Pisarevsky, S. A., Wingate, M. T. D., Li, Z. X., Wang, X. C., Tohver, E., and Kirkland, C. L., 2014, Age and paleomagnetism of the 1210Ma Gnowangerup-Fraser dyke swarm, Western Australia, and implications for late Mesoproterozoic paleogeography: Precambrian Research, vol. 246, pp. 1–15, .
Potter, D. K. and Stephenson, A., 1988, Single-domain particles in rocks and magnetic fabric analysis: Geophysical Research Letters, vol. 15, pp. 1097–1100, .
Qiu, Y., McNaughton, N. J., Groves, D. I., and Dunphy, J. M., 1999, First record of 1.2 Ga quartz dioritic magmatism in the Archaean Yilgarn Craton, Western Australia, and its significance: Australian Journal of Earth Sciences, vol. 46, pp. 421–428, .
Salminen, J., Halls, H. C., Mertanen, S., Pesonen, L. J., Vuollo, J., and Söderlund, U., 2014, Paleomagnetic and geochronological studies on Paleoproterozoic diabase dykes of Karelia, East Finland-Key for testing the Superia supercraton: Precambrian Research, vol. 244, pp. 87–99, .
Salminen, J., Oliveira, E., Piispa, E., Smirnov, A., and Trindade, R., 2019, Revisiting the paleomagnetism of the Neoarchean Uauá mafic dyke swarm, Brazil: Implications for Archean supercratons: Precambrian Research, vol. 329, pp. 108–123, .
Smirnov, A. V., Evans, D. A. D., Ernst, R. E., Söderlund, U., and Li, Z. X., 2013, Trading partners: Tectonic ancestry of southern Africa and western Australia, in Archean supercratons Vaalbara and Zimgarn: Precambrian Research, vol. 224, pp. 11–22, .
Spaggiari, C. V., Bodorkos, S., Barquero-Molina, M., Tyler, I. M., and Wingate, M. T. D., 2009, Interpreted Bedrock Geology of the South Yilgarn and of the South Yilgarn and Central Albany-Fraser Orogen, Western Australia: Geological Survey of Western Australia.
Spaggiari, C. V., Kirkland, C. L., Smithies, R. H., Wingate, M. T. D., and Belousova, E. A., 2015, Transformation of an Archean craton margin during Proterozoic basin formation and magmatism: The Albany-Fraser Orogen, Western Australia: Precambrian Research, vol. 266, pp. 440–466, .
Standing, J. G., 2008, Terrane amalgamation in the Eastern Goldfields Superterrane, Yilgarn Craton: Evidence from

tectonostratigraphic studies of the Laverton Greenstone Belt: Precambrian Research, vol. 161, pp. 114–134, .
Stark, J., Wang, X.-C., Denyszyn, S., Li, Z.-X., Rasmussen, B., Zi, J.-W., Sheppard, S., and Liu, Y., 2019, Newly identified 1.89 Ga mafic dyke swarm in the Archean Yilgarn Craton, Western Australia suggests a connection with India: Precambrian Research, vol. 329, .
Stark, J. C., Wilde, S. A., Söderlund, U., Li, Z. X., Rasmussen, B., and Zi, J.-W., 2018, First evidence of Archean mafic dykes at 2.62 Ga in the Yilgarn Craton, Western Australia: Links to cratonisation and the Zimbabwe Craton: Precambrian Research, vol. 317, pp. 1–13, .
Tarling, D. H. and Hrouda, F., 1993, Magnetic Anisotropy of Rocks, vol. 5: Springer Science & Business Media, .
Tauxe, L., Mullender, T. A. T., and Pick, T., 1996, Potbellies, wasp-waists, and superparamagnetism in magnetic hysteresis: Journal of Geophysical Research: Solid Earth, vol. 101, pp. 571–583, .
Tauxe, L., Shaar, R., Jonestrask, L., Swanson-Hysell, N. L., Minnett, R., Koppers, A. A., Constable, C. G., Jarboe, N., Gaastra, K., and Fairchild, L., 2016, PmagPy: Software package for paleomagnetic data analysis and a bridge to the Magnetics Information Consortium (MagIC) Database: Geochemistry, Geophysics, Geosystems, vol. 17, pp. 2450–2463, .
Wang, X. C., Li, Z. X., Li, J., Pisarevsky, S. A., and Wingate, M. T. D., 2014, Genesis of the 1.21 Ga Marnda Moorn large igneous province by plume-lithosphere interaction: Precambrian Research, vol. 241, pp. 85–103, .
Wilde, S., Middleton, M., and Evans, B., 2002, Terrane accretion in the southwestern Yilgarn Craton: Evidence from a deep seismic crustal profile: Precambrian Research, vol. 78, pp. 179–196, .
Wilde, S. A., 2001, Jimperding and Chittering Metamorphic Belts, Southwestern Yilgarn Craton, Western Australia – a Field Guide, vol. Record 2001/12: Geological Survey of Western Australia.
Wingate, M. T. D. and Pidgeon, R. T., 2005, The Marnda Moorn LIP, A late Mesoproterozoic Large Igneous Province in the Yilgarn Craton, Western Australia July2005 LIP of the Month. Large Igneous Provinces Commission, International Association of Volcanology and Chemistry of the Earth's Interia: http://www.largeigneousprovinces.org/05jul.
Wingate, M. T. D., Pirajno, F., and Morris, P. A., 2004, Warakurna large igneous province: A new Mesoproterozoic large igneous province in west-central Australia: Geology, vol. 32, pp. 105–108, .
Wingate, M. T. D., Pisarevsky, S. A., and Evans, D. A. D., 2002, Rodinia connections between Australia and Laurentia: No SWEAT, no AUSWUS?: Terra Nova, vol. 14, pp. 121–128, .
Wyche, S., 2007, Chapter 2.6 Evidence of Pre-3100 Ma Crust in the Youanmi and South West Terranes, and Eastern Goldfields Superterrane, of the Yilgarn Craton: *In* Developments in Precambrian Geology, vol. 15, pp. 113–123, .
Yoshihara, A. and Hamano, Y., 2004, Paleomagnetic constraints on the Archean geomagnetic field intensity obtained from komatiites of the Barberton and Belingwe greenstone belts, South Africa and Zimbabwe: Precambrian Research, vol. 131, pp. 111–142, .